Article

Current Biology

A mechanism for differential control of axonal and dendritic spiking underlying learning in a cerebellum-like circuit

Graphical abstract

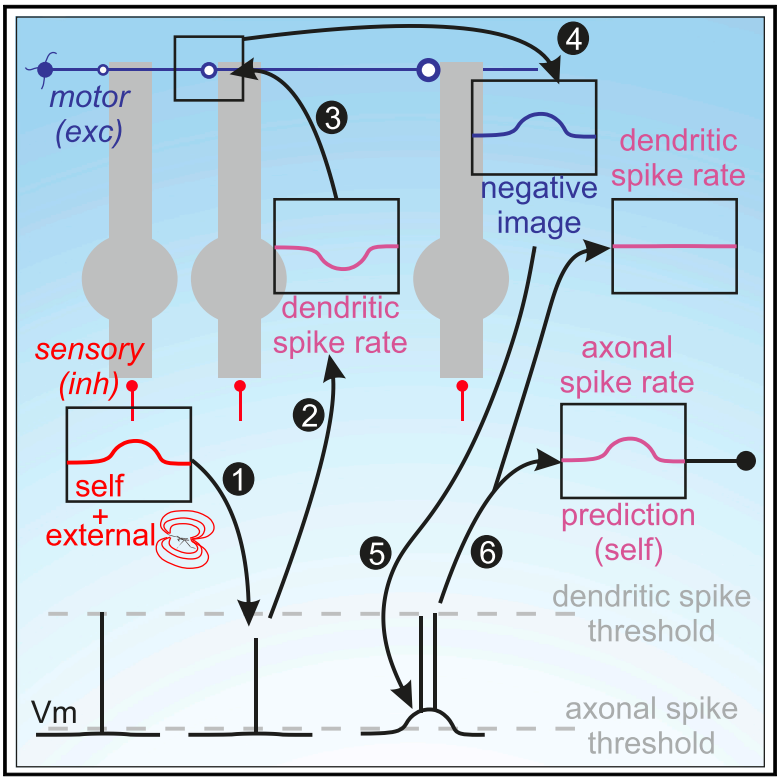

Authors

Salomon Z. Muller, L.F. Abbott, Nathaniel B. Sawtell

Correspondence

ns2635@columbia.edu

In brief

Muller et al. elucidate mechanisms for independent control over axonal and dendritic spikes by sensory input in a cerebellum-like circuit in weakly electric fish. These results provide a biophysical explanation for how predictions formed by homeostatic synaptic plasticity can be transmitted across processing stages in multi-layer circuits.

Highlights

- A biophysical basis for learning and transmitting sensory predictions is described
- Backpropagating axonal spikes trigger dendritic spikes
- Sensory inhibition controls the amplitude of backpropagating axonal spikes
- Axonal compartmentalization is critical for a learning-related computation

Muller et al., 2023, Current Biology *33*, 2657–2667
July 10, 2023
https://doi.org/10.1016/j.cub.2023.05.040

CellPress

Current Biology

CellPress

Article

A mechanism for differential control of axonal and dendritic spiking underlying learning in a cerebellum-like circuit

Salomon Z. Muller,[1] L.F. Abbott,[1,2] and Nathaniel B. Sawtell[1,3,*]
[1]Zuckerman Mind Brain Behavior Institute, Department of Neuroscience, Columbia University, New York, NY 10027, USA
[2]Department of Physiology and Cellular Biophysics, Columbia University, New York, NY 10027, USA
[3]Lead contact
*Correspondence: ns2635@columbia.edu
https://doi.org/10.1016/j.cub.2023.05.040

SUMMARY

In addition to the action potentials used for axonal signaling, many neurons generate dendritic "spikes" associated with synaptic plasticity. However, in order to control both plasticity and signaling, synaptic inputs must be able to differentially modulate the firing of these two spike types. Here, we investigate this issue in the electrosensory lobe (ELL) of weakly electric mormyrid fish, where separate control over axonal and dendritic spikes is essential for the transmission of learned predictive signals from inhibitory interneurons to the output stage of the circuit. Through a combination of experimental and modeling studies, we uncover a novel mechanism by which sensory input selectively modulates the rate of dendritic spiking by adjusting the amplitude of backpropagating axonal action potentials. Interestingly, this mechanism does not require spatially segregated synaptic inputs or dendritic compartmentalization but relies instead on an electrotonically distant spike initiation site in the axon—a common biophysical feature of neurons.

INTRODUCTION

Many classes of neurons fire both axonal and dendritic action potentials.[1–6] Whereas axonal spikes mediate inter-cellular signaling, dendritic spikes are often associated with the induction of synaptic plasticity.[7,8] This raises the possibility that two spike types allow individual neurons to control signaling and learning-related functions separately.[9–12] For this to be possible, however, synaptic inputs must be able to differentially modulate the firing of axonal and dendritic spikes. In Purkinje cells, this is accomplished by a powerful excitatory input (the climbing fiber) that is required to evoke dendritic "complex" spikes.[13] Most neurons, however, do not have such clearly specialized input and presumably rely on other mechanisms, for example, spatially localized synaptic inputs.[14,15] Here, we elucidate the biophysical basis for differential control over axonal (narrow) and dendritic (broad) spikes in a well-studied class of electrosensory lobe (ELL) interneuron known as the medium ganglion (MG) cell. In these cells, narrow spikes are initiated in the axon, have a low threshold, and are emitted at high rates (~50 Hz), whereas broad spikes are initiated in the soma or proximal apical dendrites, have a high threshold, and are emitted at low rates (~2 Hz).[16–18] Narrow spikes constitute the main signaling output of MG cells (due to their much higher rate), while broad spikes play a critical role in triggering synaptic plasticity.[19,20] As will be described below, advantageous features of this system allow the detailed biophysical interplay between narrow and broad spikes in MG cells to be directly linked to circuit and systems level function.

Weakly electric mormyrid fish use both active and passive electrolocation to detect and localize nearby objects, such as prey.[21] In active electrolocation, the fish senses modulations of its own electric organ discharge (EOD) pulses, while in the passive case, a different set of highly sensitive electroreceptors detects the minute electric fields generated by other organisms. These two systems operate simultaneously, which raises a problem for the passive system: active, self-generated EOD pulses induce large, long-lasting ringing in the passive electroreceptors that masks the responses to the external fields they are tuned to detect.[22] Extensive prior work has shown that this problem is solved in the hindbrain ELL, where information from electroreceptors is combined with a diverse array of signals, including a corollary discharge of the fish's EOD motor command, in order to cancel responses to self-generated sensory input induced by the EOD.[23–25] Electroreceptors' afferent nerve fibers project somatotopically to the deep layers of the ELL (Figure 1A, red), whereas corollary discharge signals are conveyed to a superficial (molecular) layer via a granule-cell-parallel fiber system similar to that found in the cerebellum (Figure 1A, blue).[26–28] These two input streams converge onto both MG cells and excitatory output cells. MG cells inhibit the output cells via two separate sub-circuits, discussed further in the results. EOD-induced electrosensory input alters the rate of broad spike firing in MG cells (Figure 1A, magenta dashed), thereby inducing anti-Hebbian plasticity at parallel fiber to MG cell synapses.[19,20,29] This plasticity gradually modifies the strength of the granule cell (corollary discharge) input, over minutes to hours, forming an inverted copy or "negative image" (Figure 1A, blue solid). The

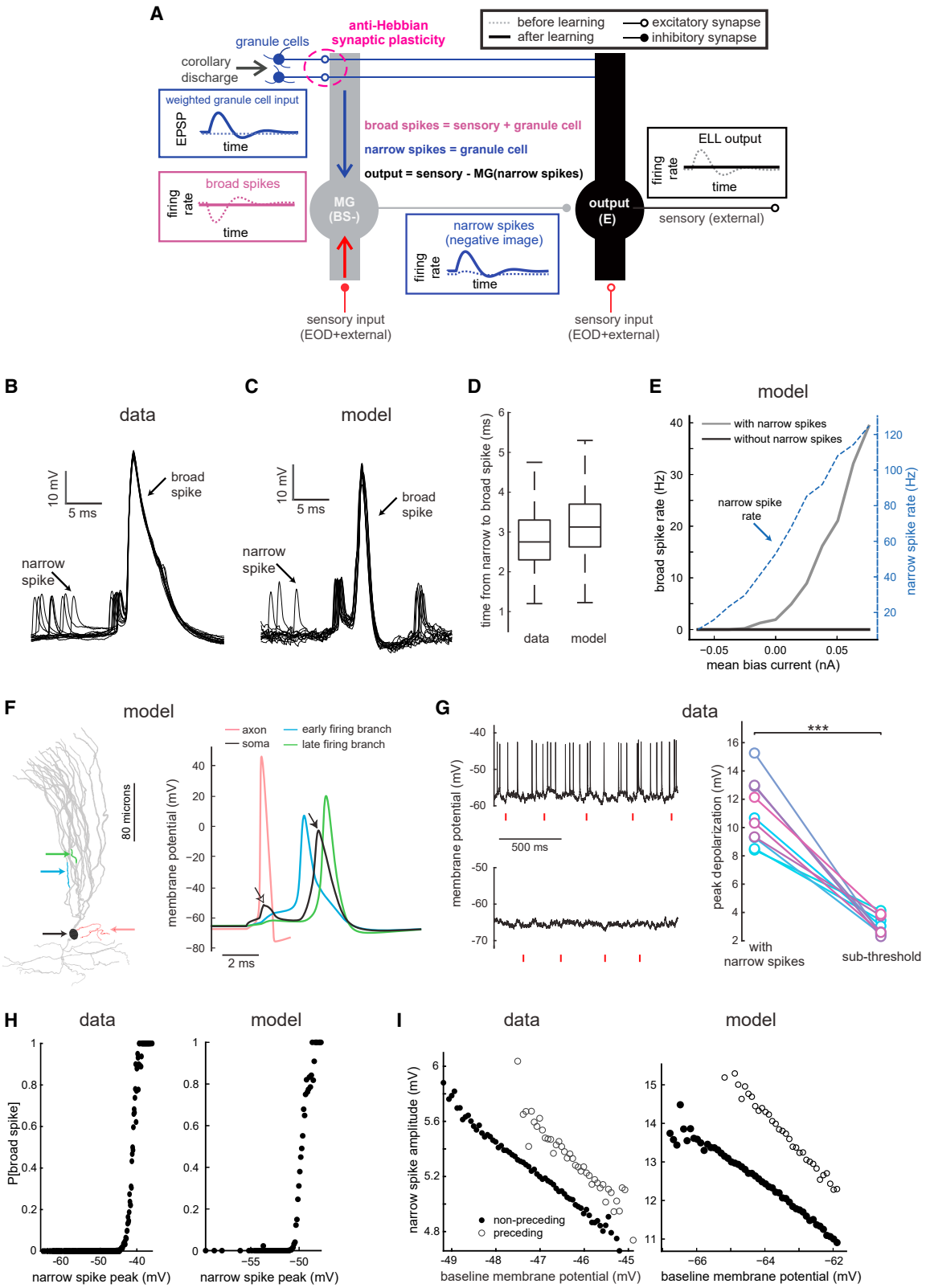

Figure 1. Backpropagating narrow spikes evoke broad spikes

(A) Schematic of negative image formation and transmission in the ELL. Electrosensory input containing both self-generated and external signals is relayed to the basilar dendrites of MG cells and output cells. For clarity, the schematic traces depict only the self-generated responses due to the fish's EOD, and note that the

(legend continued on next page)

negative image cancels the effects of EOD-induced sensory input on broad spiking, thus restoring the rate of broad spike firing to a constant (unmodulated) rate of ~2 Hz (Figure 1A, magenta solid).[26,30] *In vivo* recordings have shown (1) that negative images are also transmitted by the narrow spike output of MG cells (Figure 1A, blue solid)[12] and (2) that the resulting inhibition contributes to cancelling responses to the EOD at the output stage of the ELL (Figure 1A, right).[12,31,32] Importantly, however, these findings remain puzzling as they appear to violate basic assumptions regarding input summation. Because negative images conveyed by excitatory granule cell input (Figure 1A, blue solid) cancel the EOD-induced sensory input (Figure 1A, red dashed), the net input to the MG cell is expected to be constant and both broad and narrow spike rates are expected to be unmodulated. This scenario leaves no way for MG cells to transmit negative images to output cells. Such conflicts between learning- and signaling-related functions are not specific to the ELL but would confront any system that relies on anti-Hebbian (homeostatic) forms of plasticity to predict sensory input (see discussion).[33,34]

Here, we provide evidence that this conflict is resolved at the biophysical level by interactions between inhibitory synaptic input, backpropagating axonal action potentials, and dendritic spikes. Specifically, we reveal mechanisms that (1) allow sensory input to affect broad and narrow spikes differently and (2) allow anti-Hebbian plasticity to maintain a constant broad spike rate by enforcing cancellation while simultaneously inducing modulations in narrow spike rate that transmit sensory predictions.

RESULTS

Dendritic spikes are triggered by backpropagating axonal spikes

We analyzed previously obtained *in vivo* intracellular recordings from MG cells and constructed a multi-compartment MG cell model that recapitulates critical features of MG cell responses.[35] In the model, voltage-gated sodium and potassium channels in the apical dendrites and at the base of the axon's initial segment generate narrow axonal and broad dendritic spikes, similar to those in real MG cells (Figure 1C). Given the critical role of broad spikes in the induction of synaptic plasticity in this system, we first sought to determine how they are evoked given that MG cells lack a climbing fiber analog.[16–18] Consistent with prior studies, we observed that broad spikes are invariably preceded by a narrow spike at a characteristic interval of ~3 ms (Figures 1B, 1D, S1A, and S1B).[16,18,36] Although these preceding narrow spikes could arise simply because broad spikes have a higher threshold than narrow spikes (a large synaptic potential that crosses the higher broad spike threshold must first cross the narrow spike threshold), we hypothesized that the brief depolarization due to the backpropagating narrow spike itself may play a causal role in evoking broad spikes. To investigate this, we examined the relationship between broad and narrow spikes in the model. When input currents were adjusted to evoke the ~50 Hz narrow spike firing and ~2 Hz broad spike firing seen *in vivo*, broad spikes in the model cell were always preceded by a narrow spike at an interval of ~3 ms (Figures 1C, 1D, and S1B). Blocking narrow spikes by turning off active conductances in the axonal compartment abolished broad spike firing over a range of input strengths (Figure 1E), while injecting a brief spike-like depolarizing current into the soma (with active conductances in the axon turned off) evoked broad spikes after a similar delay (Figure S1C). These results establish a causal role for narrow spikes in evoking broad spikes in the model. Monitoring the voltage at various locations revealed that even though the axonal depolarization resulting from the narrow spike is highly attenuated by the time it reaches the soma (Figure 1F, open arrowhead), it nevertheless spreads passively into the proximal apical dendrites where it activates voltage-gated sodium and potassium channels to evoke a local dendritic spike (Figure 1F, blue). Depolarization from the local dendritic spike then propagates into other apical branches leading to additional spike initiations at multiple sites throughout the apical dendrite. These local dendritic spikes sum to produce a broad somatic spike after a delay of several milliseconds from the triggering narrow spike (Figure 1F, filled arrowhead; Video S1). Characteristics of putative apical dendritic MG cell recordings *in vivo* are consistent with the model; narrow spikes are smaller and broad spikes are

negative image can only cancel the response to the predicted, self-generated, sensory input. The dashed and solid traces depict responses before and after negative image formation. Anti-Hebbian plasticity at granule cell synapses onto MG cells sculpts motor corollary discharge input into a negative image (blue trace), which cancels the effects of the EOD on broad spike firing (magenta trace). Negative images also simultaneously modulate the rate of narrow spike firing (blue trace) via previously unknown mechanisms that are elucidated here. The ELL also contains a second, parallel sub-circuit (not shown), consisting of a second MG sub-class (termed BS+) and a second output cell sub-class (termed I-cells). This circuit is similar to the one depicted, but with the polarity of the sensory- and granule-cell-evoked neural responses reversed.

(B and C) Overlaid intracellular voltage traces from an example MG cell recorded *in vivo* (B) (also see Figure S1D) and the model cell (C).

(D) Interval between peaks of narrow and broad spikes in recorded (n = 17) and model MG cells.

(E) Effect of eliminating narrow spikes on broad spike firing in the model. Narrow spike F-I curve is also shown.

(F) Left: neurolucida reconstruction of an MG cell used to build the multi-compartment model. Arrows indicate the sites of the membrane voltage recordings depicting the process of broad spike initiation (right). Open and filled arrows indicate somatically recorded narrow and broad spikes, respectively. Voltage trace from the axon is truncated for clarity (omitted portion shows that broad spikes trigger an additional axonal spike as shown in Video S1).

(G) Left: membrane potential fluctuations in an MG cell recorded with no bias current (top) and with hyperpolarizing bias current to prevent narrow spiking (bottom). Red lines indicate the times of the fish's electric organ discharge command. Right: peak depolarization amplitudes (relative to baseline) are substantially larger with narrow spikes intact (n = 10, $p < 0.001$).

(H) Left: example MG cell recording illustrating the relationship between broad spike probability and the peak of the narrow spike immediately preceding the broad spike. Additional examples are shown in Figure S1G. Right: same display for the model cell.

(I) Narrow spike amplitude depends on the baseline membrane potential (i.e., the point from which the spike arises), but for any given baseline membrane potential, narrow spikes that precede broad spikes have, on average, a larger amplitude. One example MG cell (left) (and see Figures S1H–S1K) and results from the model cell (right). Each circle represents the average amplitude for the given baseline membrane potential.

See also Video S1.

narrower in comparison with somatic recordings (Figures S1D and S1E).

Several lines of evidence suggest a causal role for backpropagating narrow spikes in evoking broad spikes *in vivo* through a process similar to that described in the model. First, eliminating narrow spikes with hyperpolarizing current or a sodium channel blocker in the recording pipette revealed that peak somatic depolarization due to narrow spikes is much greater than that due to subthreshold input alone (Figure 1G). Second, *in vivo* (as in the model), the probability of evoking a broad spike depends strongly on the membrane potential at the peak of the recorded narrow spike (Figures 1H, S1F, and S1G). Third, *in vivo* (as in the model), narrow spikes that immediately precede a broad spike not only arise from more depolarized potentials (as would be expected based on the higher threshold for broad spikes) but also exhibit larger amplitudes than narrow spikes not preceding a broad spike (Figures 1I and S1H–S1K). Note, this analysis also shows that the amplitude of backpropagating narrow spikes depends on the baseline membrane potential, an effect seen in other systems,[3] presumably due to the voltage-dependence of the membrane conductance. Although these results do not prove a causal role for narrow spikes in evoking broad spikes, they argue against the alternative possibilities that broad spikes are evoked either by large synaptic events visible at the soma (Figure 1G) or by strong apical input that does not propagate to the soma (Figures 1H and 1I).

Sensory input modulates broad but not narrow spiking

We next examined how sensory input affects broad and narrow spike firing in the multi-compartment model. *In vivo* studies have revealed two distinct sub-classes of MG cells, which respond with opposite polarity to sensory input.[12] In BS− cells, the initial component of the response is a decrease in broad spike rate (Figure 1A), while in BS+ cells, the initial component of the response is an increase in broad spike rate. In prior work, *in vivo* responses of both MG cell sub-classes were reproduced in the model under the assumption that broad spikes in BS+ cells are evoked by dis-inhibition.[12] Because implementing this dis-inhibitory circuit adds additional complexity to the modeling, we focused on analyzing the behavior of BS− cells. For clarity, we consider constant sensory input, but we have verified that all the results we report apply to time-dependent sensory inputs matching those *in vivo* (Figures S2D and S2E).

Adding relatively weak inhibitory input to basilar dendritic compartments potently reduces the broad spike firing rate with little effect on the rate of narrow spikes (Figure 2A, inhibition), consistent with prior *in vivo* recordings.[12] Measuring membrane potential values in the somatic compartment of the model revealed that inhibition results in narrow spikes reaching less depolarized levels at their peaks (Figure 2B, red; Figure S2A), so that the broad spike threshold is rarely crossed (Figure 2B, gray and dashed line). The increased conductance due to the inhibitory input reduces the peak membrane potential by attenuating the passive spread of the narrow spike from the axon's initial segment, as seen in the small reduction in the amplitude of the narrow spike at the soma (∼0.75 mV; Figures 2C and 2E, red; Figure S2B; see STAR Methods for analytical results). The effects of inhibitory input on the baseline membrane potential and the narrow spike rate are negligible because the narrow spike threshold (∼−64 mV) is near the reversal potential for inhibition (−65 mV in the model). No further fine-tuning of parameters is required to produce the results we report and, in fact, as we show later, the basic effects can be reproduced in a simple two-compartment model.

Reconciling the effects of plasticity on broad and narrow spikes

We have shown that modulating the amplitude of backpropagating narrow spikes has a differential effect on broad and narrow spiking. We now examine the effects of plasticity on these two spike types. The dynamics of anti-Hebbian spike-timing-dependent plasticity acting on realistic granule cell corollary discharge inputs have been extensively characterized and modeled.[19,26,30] Because the focus here is on the consequences of these well-characterized plasticity dynamics on narrow and broad spike firing (rather than on the plasticity mechanism itself), we simply reproduce the known effect of this plasticity in our model rather than modeling it explicitly. In other words, we set the strengths of excitatory conductances onto apical dendrites to cancel the effects of inhibition on the broad spike rate (Figure 2A, cancellation).

As shown in the previous section, adding sensory input to an MG cell that initially received no such input temporarily lowers the broad spike rate from its baseline value. Mimicking plasticity at granule cell synapses returns the broad spike rate to this baseline value by restoring the membrane potential at the peak of the backpropagating narrow spike close to its original value (Figure 2B, cyan; Figure S2A). At the same time, the added granule cell excitatory input generated by the plasticity increased the narrow spike rate (Figure 2A, cancellation). This increase is what allows MG cells to transmit the negative image they compute to output cells of the ELL. However, the fact that after plasticity, narrow spiking—but not broad spiking—has increased, raises a question. We have shown that narrow spikes evoked broad spikes, although with a low probability given the difference in background rates (∼50 Hz for narrow and ∼2 Hz for broad spikes). After plasticity, there are more narrow spikes, but not more broad spikes. How is this possible if, as we claim, narrow spikes generate broad spikes?

We have shown that the average membrane potential at the peak of the backpropagating narrow spike is brought back to its initial, pre-input, value by plasticity. However, the reduction in the backpropagating narrow spike amplitude caused by inhibition is not reversed (Figure 2C, cyan; Figure S2B). Instead, the peak height is restored because the smaller amplitude backpropagating spike rides on top of a depolarization of the underlying membrane potential (Figures 2D and 2E, cyan; Figure S2C). This baseline depolarization is what drives the increase in narrow spike firing, thereby transmitting the negative image to downstream neurons (Figure 2A, cancellation). Analytical results suggest that the same mechanism operates in BS+ cells, under the assumption that broad spikes are evoked by dis-inhibition (Figure S2F).

An equivalent explanation for this phenomenon can be constructed by expressing the broad spike rate, R_{bs}, as the product of two factors, the probability of a narrow spike evoking a broad spike, p, and the rate of narrow spikes, r_{ns}: $R_{bs} = p \cdot r_{ns}$. The factor p reflects the functional coupling between backpropagating

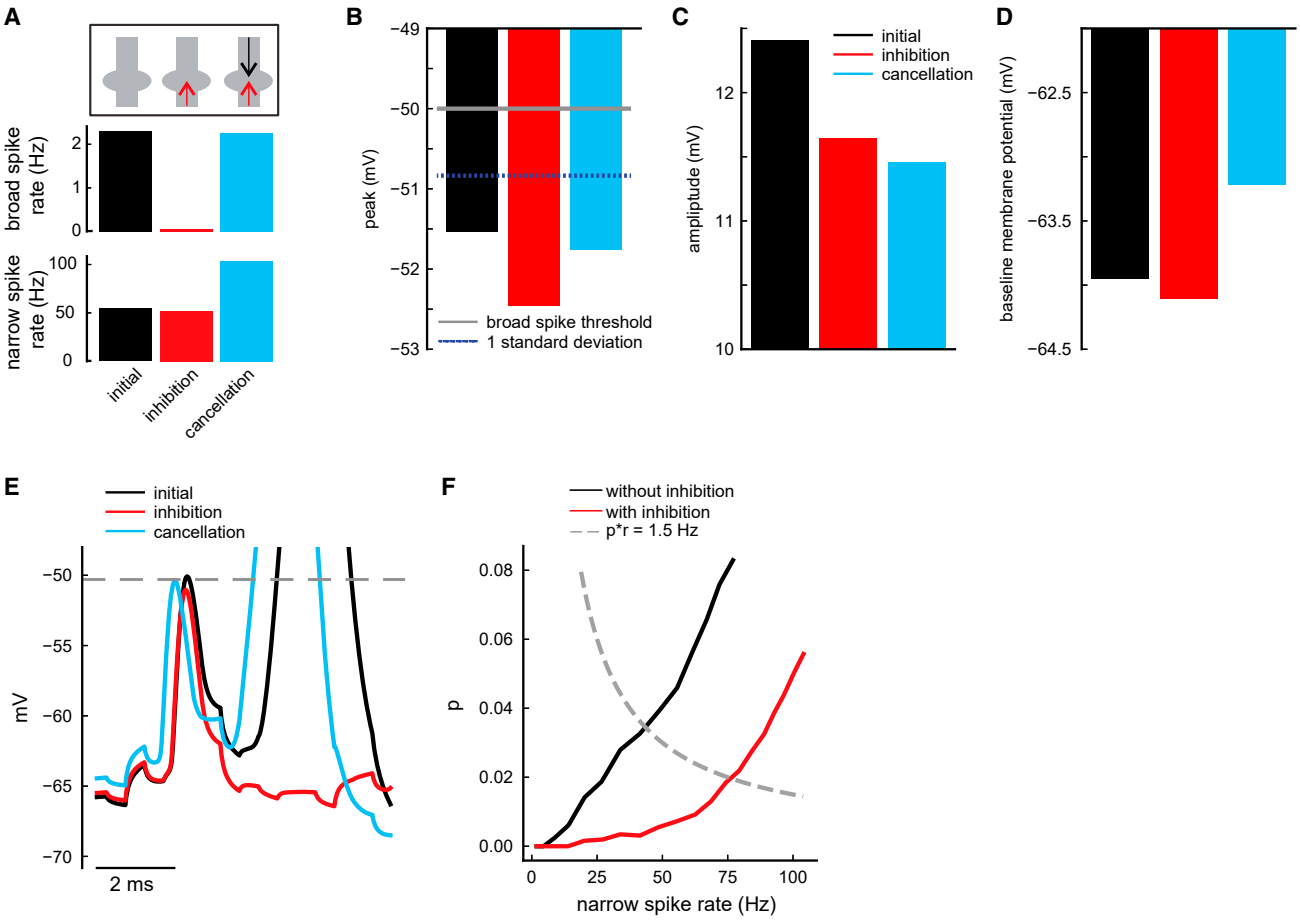

Figure 2. Biophysical model of negative image formation and transmission

(A) Narrow and broad spike rates under three conditions used to simulate the formation and transmission of negative images in the model (see main text). To simplify model analysis, we use step-like changes in sensory and corollary discharge input rather than simulating the temporal response profiles observed *in vivo* Figure S2 (Figures S2D and S2E). This is equivalent to plotting the peak of the responses schematized in Figure 1A.

(B) Peak membrane potential of backpropagating narrow spikes for the input conditions shown in (A). Gray line indicates the broad spike threshold. The distance from the gray line to the dashed blue line is approximately one standard deviation from the mean value of the membrane potential at the peak of the narrow spike (this value is similar across conditions). This illustrates that the change in the peak of the narrow spike due to sensory inhibition drives the membrane potential far from the threshold, explaining the large reduction in broad spike rate.

(C) Backpropagating narrow spike amplitudes for the input conditions shown in (A).

(D) Baseline membrane potentials for the input conditions shown in (A).

(E) Example voltage traces from the model illustrating how membrane potential depolarization (cyan) allows narrow spikes to cross the threshold for evoking a broad spike (dashed line), despite the reduction in narrow spike amplitude due to inhibition (red).

(F) Inhibition (red) reduces probability of evoking a broad spike (p), such that an increase in narrow spike rate is required to restore the broad spike rate to equilibrium (dashed line). This increase is proportional to the negative image. Equilibria for the two conditions are where the dashed and solid curves cross. See also Figure S3.

narrow spikes and broad spikes (similar to the "safety factor" described in classical studies of initial segment-somatodendritic spike coupling[37–40]). Sensory input selectively affects the broad spike rate by reducing the value of p. Although narrow spike peak voltage is the dominant factor affecting p (Figure 1H), other factors may also contribute (Figure S3). Specifically, suppose that the broad spike rate $R_{bs} = p \cdot r_{ns}$ is at its equilibrium value in the absence of sensory input, with $p = p_0$. Introducing inhibition due to sensory input reduces p, causing the broad spike rate to decrease. Synaptic plasticity restores the broad spike rate by returning $p \cdot r_{ns}$, and thus R_{bs}, back to its equilibrium value (Figure 2F, dashed line). However, through this process p is not restored to its previous value p_0, but instead remains smaller than p_0. Thus, the broad spike rate is restored to its equilibrium value despite an increase in r_{ns}, the narrow spike rate (Figure 2F).

Negative image formation and transmission *in vivo*

The model makes two key predictions regarding negative image generation and transmission that we tested using *in vivo* intracellular recordings from both BS− and BS+ type MG cells obtained previously.[12] Note that for BS+ cells, both the sign of the broad spike response to the sensory input and the sign of the negative image are reversed. First, sensory input is hypothesized to decrease (in BS− cells) or increase (in BS+ cells) the amplitude

of narrow spikes recorded in the soma. Second, the plasticity of granule cell (corollary discharge) input is hypothesized to cancel the effects of sensory input on the broad spike rate by changing the underlying membrane potential (rather than by reversing the effects of sensory input on narrow spike amplitude). Comparing narrow spike amplitudes in time windows when broad spike firing was modulated by an electrosensory stimulus versus control windows, revealed that the sensory stimuli that suppressed broad spiking reduced the amplitude of backpropagating narrow spikes, while stimuli that enhanced broad spiking increased this amplitude (Figures 3A–3C and S4A). These results directly support the first hypothesis.

To test prediction 2 concerning the changes in baseline membrane potential, we examined narrow spike amplitudes during the formation of negative images induced by pairing an electrosensory stimulus with the motor command that discharges the electric organ.[31] These experiments utilize an immobilized preparation in which emission of the EOD is blocked but in which fish continue to spontaneously emit the EOD motor command (which can be recorded extracellularly near the tail) at a rate of ~2–5 Hz.[31] This analysis was only possible for BS+ cells because of the faster time course of cancellation in these cells and the technical difficulty of maintaining stable intracellular recordings of sufficient quality to analyze changes in spike amplitude.[12] As expected, cancellation of sensory-evoked increases in broad spike firing was driven by a temporally specific hyperpolarization of the underlying membrane potential (Figure 3D, inset). Importantly, sensory-evoked changes in narrow spike amplitude were not reversed as negative images formed, a critical feature for our model of negative image transmission (Figures 3D, S4D, and S4E). In fact, the amplitude of backpropagating narrow spikes actually increased due to the prominent inverse correlation of the narrow spike amplitude and the baseline membrane potential (Figure 1I). This effect amplifies the mechanism identified in the model, leading to even more robust negative image transmission by narrow spikes (Figures S4F and S4G). Defining ΔAmp as the change in narrow spike amplitude due to sensory input and S as the slope of the relationship between narrow spike amplitude and the baseline membrane potential (Figures S4B and S4C), the learned negative image is equal to $-\Delta Amp/(1 + S)$. Our data suggest a value for S of ~−4.1% (1/mV) (Figure S4B; see STAR Methods for the derivation of this value), which corresponds to −0.5 for a typical 12-mV narrow spike recorded in the soma. Hence, the negative image generated by a 3% narrow spike amplitude change (Figure 3C) is expected to be 0.35 mV/(1 − 0.5) = 0.7 mV. Based on measured dependence of the narrow spike firing rate on membrane potential (Figures 3E and 3F), this amounts to an ~25-Hz change in narrow spike rate, which is comparable in magnitude to negative images recorded *in vivo*.[12]

Axonal, but not dendritic, compartmentalization is required for MG cell function

The differential effect of sensory input on broad and narrow spikes might suggest that spatial targeting of synaptic inputs onto MG cells is essential for generating and transmitting negative images. We tested this by varying the location of the inhibitory sensory input in the model. Surprisingly, sensory inhibition onto the proximal apical dendrites (Figure 4A) or soma (Figure 4B) yielded similar model performance as did sensory inhibition onto basilar dendrites (Figure 2A). In both cases, sensory inhibition robustly decreased broad spike firing with little effect on narrow spike firing (Figures 4A and 4B, inhibition), and the addition of excitatory granule cell (corollary discharge) input to the apical dendrites cancelled the effects of sensory input on the broad spike rate while simultaneously modulating narrow spike output (Figures 4A and 4B, cancellation). Furthermore, if a mixture of excitatory and relatively strong inhibitory sensory inputs are delivered to the basilar dendrites, the narrow spike firing rate is also increased (due to an increase in baseline membrane potential), while broad spike firing is decreased (due to a decrease in narrow spike amplitude) (Figure 4C), matching prior *in vivo* observations.[12] These results suggest that neither spatially segregated synaptic inputs nor dendritic compartmentalization are strictly required for differential control over broad and narrow spikes.

To test this further, we constructed a simple conductance-based integrate-and-fire model with only two compartments, representing an axon and a soma. In this model, a realistic shaped action potential is inserted in the axon when the narrow spike threshold is reached and then backpropagates to the soma. When the soma reaches a high threshold value, this results in the firing of a broad spike (Figure 4E; STAR Methods). Remarkably, the same qualitative results described for the morphologically realistic multi-compartment model were reproduced by the attenuation of the backpropagating axonal narrow spike in the somatic compartment (Figures 4D–4F). Although this result in no way excludes important functional roles for the numerous morphological, synaptic, and biophysical specializations of real MG cells, it suggests a minimal set of essential biophysical requirements for differential control of narrow and broad spiking.

DISCUSSION

An essential role for axonal compartmentalization

An action potential that arrives at the soma highly attenuated might seem an unlikely candidate for impacting dendrites. We find, to the contrary, that the small size of backpropagating axonal spikes in MG cells makes them susceptible to modulation and therefore an ideal candidate for flexibly controlling dendritic events. Importantly, the amplitude of backpropagating action potentials is much more sensitive to synaptic input[5,40,41] than rates of action potential generation. This provides a mechanism for precise and, importantly, differential control of axonal and dendritic spikes that supports their separate functions. Whereas discussion of neuronal compartmentalization typically focuses on dendritic structure,[7,15,42] our work provides a case in which the separation of the axon from the soma and dendrites is the essential element. Although in our models this separation is based on the high resistance between axonal and somatic compartments and the generation of the axonal spike at the base of the axon initial segment, additional specializations (and potential sites of regulation) are likely to exist in real cells.[43] For example, studies of medium superior olive neurons in the mammalian auditory brainstem provide evidence that the precise subcellular localization and inactivation properties of voltage-gated sodium channels contribute to the electrical isolation of the axon's initial segment from the soma and dendrites.[44,45]

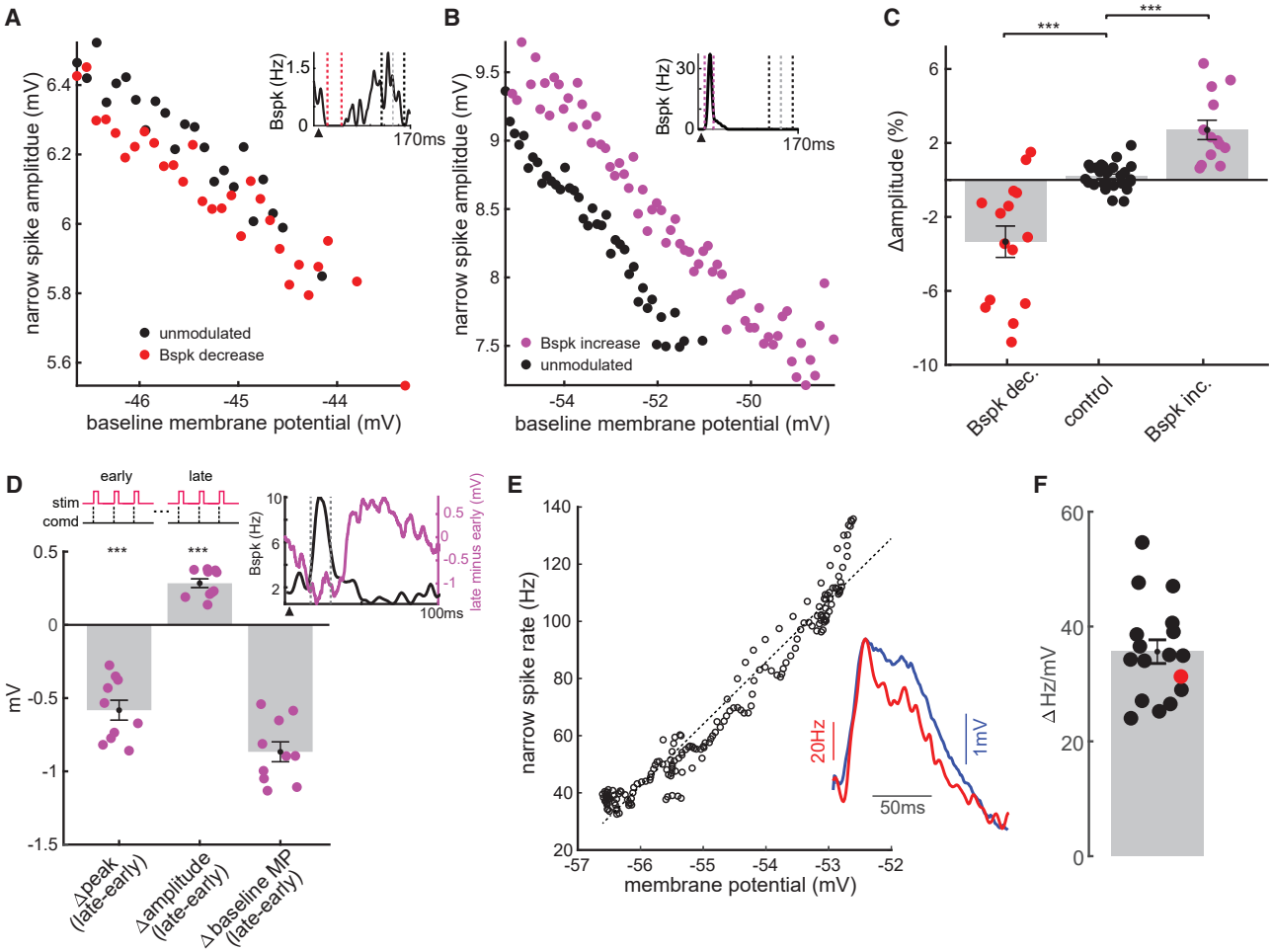

Figure 3. Negative image formation and transmission *in vivo*

(A) Example BS− MG cell illustrating a decrease in the backpropagating narrow spike amplitude in a time window when broad spike firing is transiently decreased by an electrosensory stimulus (red) compared with a window in which the broad spike rate is not modulated (black). Inset here and in (B) identifies these analysis windows and shows the average broad spike response to the electrosensory stimulus (black triangle).

(B) Example BS+ MG cell illustrating an increase in the backpropagating narrow spike amplitude in a time window when broad spike firing was transiently increased by an electrosensory stimulus (magenta).

(C) Summary of the effects of sensory stimuli on narrow spike amplitude across MG cells (n = 15 decrease, n = 13 increase, $p < 0.001$). Middle bar (control) shows results of analysis comparing amplitudes in two windows in which broad spike rates were not modulated (the two windows are separated by the gray dashed line in insets A and B).

(D) Changes in membrane potential at the peak of the narrow spike (Δpeak), narrow spike amplitude (Δamplitude), and the baseline membrane potential preceding narrow spikes (Δbaseline MP) during pairing (~4 min) of an electrosensory stimulus with the electric organ discharge motor command (comd) to induce negative image formation and sensory cancellation in BS+ cells (n = 10). Inset right, traces from an example cell illustrating the initial sensory-evoked increase in broad spike firing (black, average of first 100 paired trials) along with the resulting change in the membrane potential (with spikes removed), which forms an approximate negative image of the effects of the paired sensory input on broad spike firing (magenta, average of final 100 minus first 100 paired trials). Inset left, illustration of the pairing paradigm.

(E) Narrow spike rate versus membrane potential plotted for one example cell. Dashed line is the linear fit. Inset, trial-averaged membrane potential (with spike removed) and corresponding narrow spike rate for the same cell.

(F) Average slope of narrow spikes to membrane potential changes across MG cells (n = 17) calculated based on the range of the curves shown in (E). The red dot corresponds to the example cell in (E).

See also Figure S4.

Limitations of the study and future directions

We posit a key functional role for small (<1 mV) changes in backpropagating narrow spike amplitude. Measuring such changes with single microelectrode recordings *in vivo* is challenging and does not directly reveal the attenuation of the spatial spread of depolarization that is hypothesized to underlie the effects we describe. Direct measurements may be possible in the future as high-speed *in vivo* voltage imaging technologies become more refined. One goal for future modeling work is to identify biophysical features that amplify the effects of sensory input on narrow spike backpropagation and/or reduce noise. Although such effects may not be visible in somatic recordings

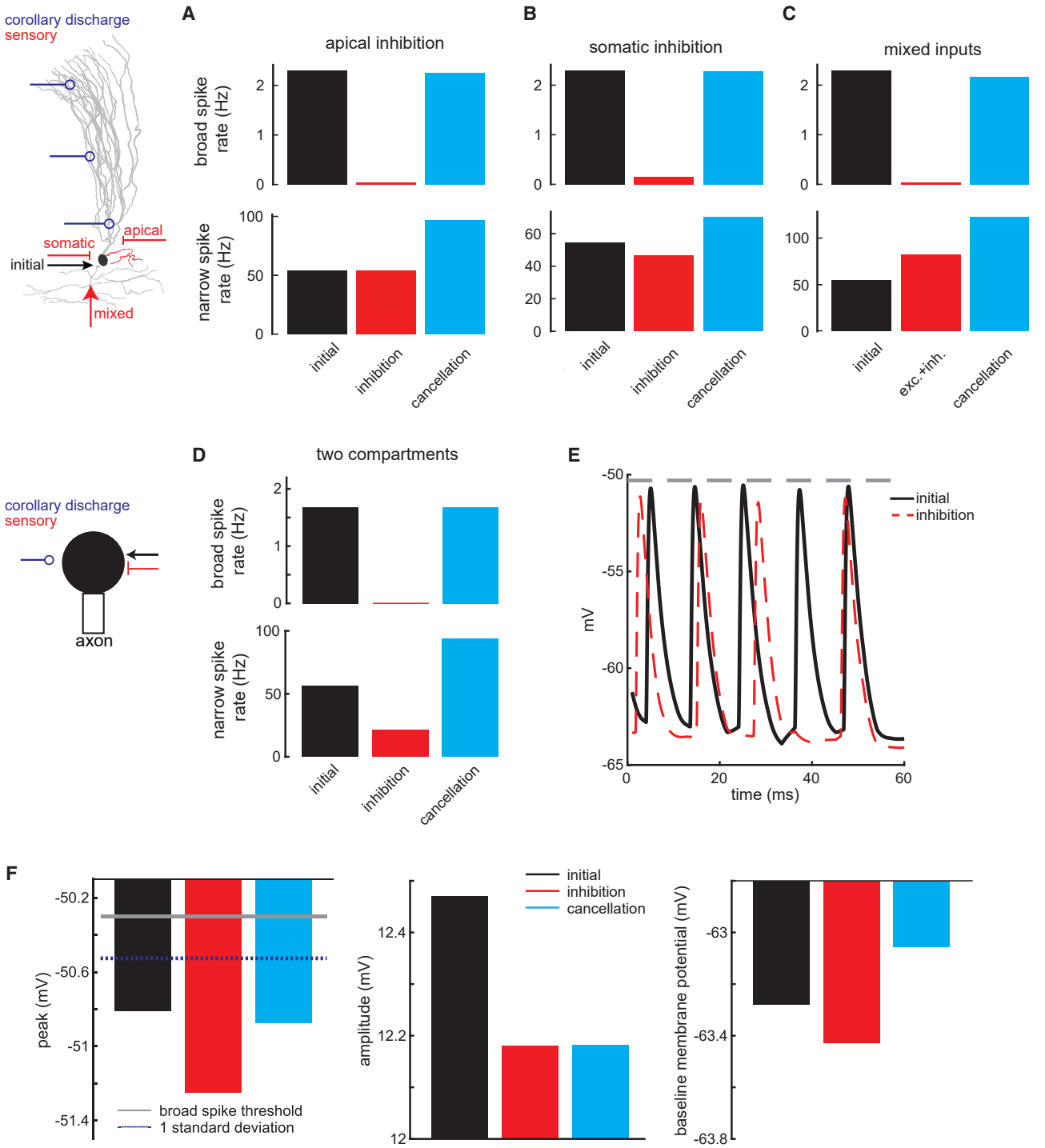

Figure 4. Negative image formation and transmission does not require dendritic compartmentalization

Left: schematic indicates locations of corollary discharge (blue) and sensory (red) inputs used in the different simulation conditions (A–C). Black arrow (initial) indicates location of inputs used to establish *in vivo*-like baseline rates of narrow and broad spike firing.

(A and B) Inhibition onto proximal apical dendrites (A) or soma (B) results in the formation and transmission of negative images in the multi-compartment model.

(C) A mixture of excitatory and inhibitory inputs decreases the firing rate of broad spikes while increasing narrow spike firing. Cancellation of broad spike inhibition results in a further increase of narrow spike firing.

(legend continued on next page)

and were not systematically analyzed here, we note that noise due to background synaptic input in the multi-compartment model is comparable to (or larger) than in somatic recording from MG cells (Figure 1B). It is also important to consider that negative images themselves are relatively small at the level of the subthreshold membrane (typically <1.5 mV)[12] and that their physiological effects are significantly amplified at the level of axonal spike generation (Figures 3E and 3F).

One goal for future studies is to characterize the circuitry within the ELL that transmits sensory input (the "target" for learning in the ELL) to different sub-classes of MG and output cells. Excitatory afferent nerve fibers conveying input from passive electroreceptors on the skin terminate in the deep layers of the ELL. Although their exact termination patterns are unknown, they likely include the basilar dendrites of MG and output cells as well as a large population of small interneurons, known as granular cells, with diverse axonal and dendritic morphology.[46] Interestingly, most granular cells appear to be inhibitory,[47,48] providing a potential anatomical substrate for the inhibitory and dis-inhibitory control over broad spikes that is critical for the mechanisms proposed here. A second goal is to characterize recurrent inhibitory connections between MG cells.[46] The present results suggest that the impact of such recurrent connections on sensory cancellation will depend not only on the structure of the connectivity between the two MG sub-classes but also on its relative impact on broad versus narrow spikes. Although our compartmental modeling indicates that inhibition targeted to the soma or basilar dendrites selectively affects broad spikes, the axon's initial segment is also a common target of inhibition that we have yet to explore in the model. Serial section electron microscopy is currently being used to map ELL circuitry at the high level of resolution required to address these issues.

Implications for other systems

The convergent evolution of cerebellum-like structures in different vertebrate groups allows for a comparative perspective on the present findings. Anti-Hebbian forms of plasticity at parallel fiber synapses are present in all cerebellum-like structures that have been examined.[24,27] Some cerebellum-like structures, such as the ELL of South American gymnotiform fish and the dorsal octavolateral nucleus of elasmobranchs, appear to lack MG cell analogs. In these structures, the main site of anti-Hebbian plasticity is at parallel fiber synapses onto glutamatergic output neurons.[23,49–51] Because negative images cancel sensory responses cell autonomously in these systems (i.e., within the output neurons themselves), separate control over axonal and dendritic spikes is not needed. Interestingly, a different form of coupling between axonal and dendritic spikes has been described for output neurons of the gymnotid ELL. In these cells, backpropagating axonal spikes generate a depolarizing afterpotential that triggers the dendritic spike bursts required for synaptic plasticity induction.[52] Regulation of this coupling by synaptic input has been implicated in novelty detection[53] and gain control.[54] Cartwheel cells in the mammalian dorsal cochlear nucleus, on the other hand, exhibit a number of striking similarities with MG cells, including anti-Hebbian spike-timing-dependent plasticity at parallel fiber synapses and distinct axonal and dendritic spikes.[55–57] Prior work has provided evidence for the cancellation of self-generated sounds in output cells of the dorsal cochlear nucleus.[58] However, as cartwheel cells lack direct auditory nerve input (equivalent to the electrosensory input to the basilar dendrites of MG cells), additional studies are required to determine whether they generate negative images of predictable auditory input. Finally, in both the mormyrid ELL and the dorsal cochlear nucleus, synaptic plasticity exists both at granule cell synapses onto inhibitory Purkinje-like cells and excitatory output cells. The existence of multiple sites of synaptic plasticity is also well-characterized in the cerebellum itself.[59] Understanding whether and how multiple sites of plasticity improve sensory cancellation in the mormyrid ELL is an important goal for future work.

Anti-Hebbian plasticity provides a powerful mechanism for generating predictions of synaptic input. However, because the stability and accuracy of anti-Hebbian learning relies on a cancellation process, such plasticity seemingly precludes the transmission of learned signals to other neurons or processing stages. Anti-Hebbian and related homeostatic forms of plasticity have been reported in the striatum[60] and neocortex[61,62] and hence may be involved in predictive processing outside of cerebellum-like structures. For example, predictive coding models of the sensory cortex posit that pyramidal neurons compute sensory prediction errors by comparing bottom-up sensory input with top-down predictions transmitted from higher cortical regions.[63] Although anti-Hebbian plasticity at inhibitory synapses onto pyramidal cells is hypothesized to underlie the computation of prediction errors in sensory cortical neurons,[33,34] the problem of how the predictions themselves are generated and transmitted between cortical layers or regions remains to be addressed. Our studies of MG cells suggest that this problem can potentially be resolved by an individual neuron endowed with anti-Hebbian plasticity and separate axonal and somatodendritic sites of action potential initiation. If the input to be predicted is conveyed via synaptic inhibition (dis-inhibition), it can alter the dendritic spike rate without substantially impacting the axonal spike rate by reducing (increasing) the amplitude of a passively backpropagating axonal spike. If anti-Hebbian plasticity is a function of the presynaptic input and the dendritic spike rate, the learned signal is not cancelled by the sensory input but, rather, can be effectively transmitted via changes in the axonal spike rate. Given its minimal biophysical requirements, core features of this mechanism could be widely used to transmit learned predictive signals.

STAR★METHODS

Detailed methods are provided in the online version of this paper and include the following:

(D) Formation and transmission of negative images can also be achieved in a simplified two-compartment model in which all the inputs are at the soma (left diagram).
(E) Trace from the two-compartment model showing the reduction of backpropagating narrow spike amplitude by inhibitory input. Dashed line is the broad spike threshold.
(F) Mechanism of negative image formation and transmission in the two-compartment model is the same as in the realistic model (cf. Figures 2B–2D).

SUPPLEMENTAL INFORMATION

Supplemental information can be found online at https://doi.org/10.1016/j.cub.2023.05.040.

ACKNOWLEDGMENTS

This work was supported by grants from the NIH (NS075023) and Irma T. Hirschl Trust to N.B.S., by a grant from the NIH (NS118448) to N.B.S. and L.F.A., and by a grant from the Swartz Foundation to S.Z.M. L.F.A. was further supported by the Gatsby and Simons Foundations and by NSF NeuroNex award DBI-1707398.

AUTHOR CONTRIBUTIONS

Conceptualization, N.B.S., S.Z.M., and L.F.A.; investigation, N.B.S.; data curation, S.Z.M. and N.B.S.; formal analysis, S.Z.M. and L.F.A.; software, S.Z.M.; resources, S.Z.M.; writing – original draft, N.B.S., L.F.A., and S.Z.M.; writing – review & editing, N.B.S., L.F.A., and S.Z.M.; funding acquisition, N.B.S. and L.F.A.

DECLARATION OF INTERESTS

The authors declare no competing interests.

Received: February 24, 2023
Revised: April 6, 2023
Accepted: May 17, 2023
Published: June 12, 2023

REFERENCES

1. Spruston, N., Schiller, Y., Stuart, G., and Sakmann, B. (1995). Activity-dependent action potential invasion and calcium influx into hippocampal CA1 dendrites. Science *268*, 297–300.
2. Stuart, G.J., and Sakmann, B. (1994). Active propagation of somatic action potentials into neocortical pyramidal cell dendrites. Nature *367*, 69–72.
3. Grace, A.A., and Bunney, B.S. (1983). Intracellular and extracellular electrophysiology of nigral dopaminergic-neurons. 2. Action-potential generating mechanisms and morphological correlates. Neuroscience *10*, 317–331. https://doi.org/10.1016/0306-4522(83)90136-7.
4. Häusser, M., Stuart, G., Racca, C., and Sakmann, B. (1995). Axonal initiation and active dendritic propagation of action potentials in susbstantia nigra neurons. Neuron *15*, 637–647.
5. Llinás, R., Nicholson, C., Freeman, J.A., and Hillman, D.E. (1968). Dendritic spikes and their inhibition in alligator Purkinje cells. Science *160*, 1132–1135. https://doi.org/10.1126/science.160.3832.1132.
6. Spencer, W.A., and Kandel, E.R. (1961). Electrophysiology of hippocampal neurons: Iv. Fast prepotentials. J. Neurophysiol. *24*, 272–285. https://doi.org/10.1152/jn.1961.24.3.272.
7. London, M., and Häusser, M. (2005). Dendritic computation. Annu. Rev. Neurosci. *28*, 503–532. https://doi.org/10.1146/annurev.neuro.28.061604.135703.
8. Magee, J.C., and Grienberger, C. (2020). Synaptic plasticity forms and functions. Annu. Rev. Neurosci. *43*, 95–117. https://doi.org/10.1146/annurev-neuro-090919-022842.
9. Marblestone, A.H., Wayne, G., and Kording, K.P. (2016). Toward an integration of deep learning and neuroscience. Front. Comput. Neurosci. *10*, 94. https://doi.org/10.3389/fncom.2016.00094.
10. Richards, B.A., and Lillicrap, T.P. (2019). Dendritic solutions to the credit assignment problem. Curr. Opin. Neurobiol. *54*, 28–36. https://doi.org/10.1016/j.conb.2018.08.003.
11. Schiess, M., Urbanczik, R., and Senn, W. (2016). Somato-dendritic synaptic plasticity and error-backpropagation in active dendrites. PLoS Comput. Biol. *12*, e1004638. https://doi.org/10.1371/journal.pcbi.1004638.
12. Muller, S.Z., Zadina, A.N., Abbott, L.F., and Sawtell, N.B. (2019). Continual learning in a multi-layer network of an electric fish. Cell *179*, 1382–1392.e10.
13. Schmolesky, M.T., Weber, J.T., De Zeeuw, C.I., and Hansel, C. (2002). The making of a complex spike: ionic composition and plasticity. Ann. NY Acad. Sci. *978*, 359–390.
14. Häusser, M., and Mel, B. (2003). Dendrites: bug or feature? Curr. Opin. Neurobiol. *13*, 372–383. https://doi.org/10.1016/S0959-4388(03)00075-8.
15. Major, G., Larkum, M.E., and Schiller, J. (2013). Active properties of neocortical pyramidal neuron dendrites. Annu. Rev. Neurosci. *36*, 1–24. https://doi.org/10.1146/annurev-neuro-062111-150343.
16. Bell, C.C., Caputi, A., and Grant, K. (1997). Physiology and plasticity of morphologically identified cells in the mormyrid electrosensory lobe. J. Neurosci. *17*, 6409–6423.
17. Engelmann, J., van den Burg, E., Bacelo, J., de Ruijters, M., Kuwana, S., Sugawara, Y., and Grant, K. (2008). Dendritic backpropagation and synaptic plasticity in the mormyrid electrosensory lobe. J. Physiol. Paris *102*, 233–245.
18. Grant, K., Sugawara, Y., Gómez, L., Han, V.Z., and Bell, C.C. (1998). The mormyrid electrosensory lobe *in vitro*: physiology and pharmacology of cells and circuits. J. Neurosci. *18*, 6009–6025.
19. Bell, C.C., Han, V.Z., Sugawara, Y., and Grant, K. (1997). Synaptic plasticity in a cerebellum-like structure depends on temporal order. Nature *387*, 278–281.
20. Han, V.Z., Grant, K., and Bell, C.C. (2000). Reversible associative depression and nonassociative potentiation at a parallel fiber synapse. Neuron *27*, 611–622.
21. Nelson, M.E. (2011). Electric fish. Curr. Biol. *21*, R528–R529. https://doi.org/10.1016/j.cub.2011.03.045.
22. Bell, C.C., and Russell, C.J. (1978). Effect of electric organ discharge on ampullary receptors in a mormyrid. Brain Res. *145*, 85–96.
23. Bell, C., Bodznick, D., Montgomery, J., and Bastian, J. (1997). The generation and subtraction of sensory expectations within cerebellum-like structures. Brain Behav. Evol. *50* (*Suppl 1*), 17–31.
24. Bell, C.C., Han, V., and Sawtell, N.B. (2008). Cerebellum-like structures and their implications for cerebellar function. Annu. Rev. Neurosci. *31*, 1–24.
25. Sawtell, N.B. (2017). Neural mechanisms for predicting the sensory consequences of behavior: insights from electrosensory systems. Annu. Rev. Physiol. *79*, 381–399. https://doi.org/10.1146/annurev-physiol-021115-105003.

26. Kennedy, A., Wayne, G., Kaifosh, P., Alviña, K., Abbott, L.F., and Sawtell, N.B. (2014). A temporal basis for predicting the sensory consequences of motor commands in an electric fish. Nat. Neurosci. *17*, 416–422.

27. Bell, C.C. (2002). Evolution of cerebellum-like structures. Brain Behav. Evol. *59*, 312–326.

28. Bell, C.C., Finger, T.E., and Russell, C.J. (1981). Central connections of the posterior lateral line lobe in mormyrid fish. Exp. Brain Res. *42*, 9–22.

29. Bell, C.C., Caputi, A., Grant, K., and Serrier, J. (1993). Storage of a sensory pattern by anti-Hebbian synaptic plasticity in an electric fish. Proc. Natl. Acad. Sci. USA *90*, 4650–4654.

30. Roberts, P.D., and Bell, C.C. (2000). Computational consequences of temporally asymmetric learning rules: II. sensory image cancellation. J. Comput. Neurosci. *9*, 67–83.

31. Bell, C.C. (1981). An efference copy which is modified by reafferent input. Science *214*, 450–453.

32. Enikolopov, A.G., Abbott, L.F., and Sawtell, N.B. (2018). Internally generated predictions enhance neural and behavioral detection of sensory stimuli in an electric fish. Neuron *99*, 135–146.e3. https://doi.org/10.1016/j.neuron.2018.06.006.

33. Hertäg, L., and Sprekeler, H. (2020). Learning prediction error neurons in a canonical interneuron circuit. eLife *9*, e57541. https://doi.org/10.7554/eLife.57541.

34. Keller, G.B., and Mrsic-Flogel, T.D. (2018). Predictive processing: a canonical cortical computation. Neuron *100*, 424–435. https://doi.org/10.1016/j.neuron.2018.10.003.

35. Roberts, P.D., and Leen, T.K. (2010). Anti-Hebbian spike-timing-dependent plasticity and adaptive sensory processing. Front. Comput. Neurosci. *4*, 156. https://doi.org/10.3389/fncom.2010.00156.

36. Sawtell, N.B., Williams, A., and Bell, C.C. (2007). Central control of dendritic spikes shapes the responses of Purkinje-like cells through spike timing-dependent synaptic plasticity. J. Neurosci. *27*, 1552–1565.

37. Coombs, J.S., Curtis, D.R., and Eccles, J.C. (1957). The generation of impulses in motoneurones. J. Physiol. *139*, 232–249. https://doi.org/10.1113/jphysiol.1957.sp005888.

38. Coombs, J.S., Curtis, D.R., and Eccles, J.C. (1957). The interpretation of spike potentials of motoneurones. J. Physiol. *139*, 198–231. https://doi.org/10.1113/jphysiol.1957.sp005887.

39. Fuortes, M.G., Frank, K., and Becker, M.C. (1957). Steps in the production of motoneuron spikes. J. Gen. Physiol. *40*, 735–752. https://doi.org/10.1085/jgp.40.5.735.

40. Renshaw, B. (1942). Effects of presynaptic volleys on spread of impulses over the soma of the motoneuron. J. Neurophysiol. *5*, 235–243. https://doi.org/10.1152/jn.1942.5.3.235.

41. Tsubokawa, H., and Ross, W.N. (1996). IPSPs modulate spike backpropagation and associated [Ca2+]I changes in the dendrites of hippocampal CA1 pyramidal neurons. J. Neurophysiol. *76*, 2896–2906. https://doi.org/10.1152/jn.1996.76.5.2896.

42. Stuart, G.J., and Spruston, N. (2015). Dendritic integration: 60 years of progress. Nat. Neurosci. *18*, 1713–1721. https://doi.org/10.1038/nn.4157.

43. Höfflin, F., Jack, A., Riedel, C., Mack-Bucher, J., Roos, J., Corcelli, C., Schultz, C., Wahle, P., and Engelhardt, M. (2017). Heterogeneity of the axon initial segment in interneurons and pyramidal cells of rodent visual cortex. Front. Cell. Neurosci. *11*, 332. https://doi.org/10.3389/fncel.2017.00332.

44. Ko, K.W., Rasband, M.N., Meseguer, V., Kramer, R.H., and Golding, N.L. (2016). Serotonin modulates spike probability in the axon initial segment through HCN channels. Nat. Neurosci. *19*, 826–834. https://doi.org/10.1038/nn.4293.

45. Scott, L.L., Mathews, P.J., and Golding, N.L. (2010). Perisomatic voltage-gated sodium channels actively maintain linear synaptic integration in principal neurons of the medial superior olive. J. Neurosci. *30*, 2039–2050. https://doi.org/10.1523/JNEUROSCI.2385-09.2010.

46. Meek, J., Grant, K., and Bell, C. (1999). Structural organization of the mormyrid electrosensory lateral line lobe. J. Exp. Biol. *202*, 1291–1300.

47. Hollmann, V., Engelmann, J., and Gómez-Sena, L. (2016). A quest for excitation: theoretical arguments and immunohistochemical evidence of excitatory granular cells in the ELL of Gnathonemus petersii. J. Physiol. Paris *110*, 190–199. https://doi.org/10.1016/j.jphysparis.2016.10.008.

48. Bell, C.C., Meek, J., and Yang, J.Y. (2005). Immunocytochemical identification of cell types in the mormyrid electrosensory lobe. J. Comp. Neurol. *483*, 124–142.

49. Bodznick, D., Montgomery, J.C., and Carey, M. (1999). Adaptive mechanisms in the elasmobranch hindbrain. J. Exp. Biol. *202*, 1357–1364.

50. Nelson, M.E., and Paulin, M.G. (1995). Neural simulations of adaptive reafference suppression in the elasmobranch electrosensory system. J. Comp. Physiol. A *177*, 723–736.

51. Bol, K., Marsat, G., Harvey-Girard, E., Longtin, A., and Maler, L. (2011). Frequency-tuned cerebellar channels and burst-induced LTD lead to the cancellation of redundant sensory inputs. J. Neurosci. *31*, 11028–11038.

52. Turner, R.W., Maler, L., Deerinck, T., Levinson, S.R., and Ellisman, M.H. (1994). TTX-sensitive dendritic sodium channels underlie oscillatory discharge in a vertebrate sensory neuron. J. Neurosci. *14*, 6453–6471.

53. Marsat, G., and Maler, L. (2012). Preparing for the unpredictable: adaptive feedback enhances the response to unexpected communication signals. J. Neurophysiol. *107*, 1241–1246. https://doi.org/10.1152/jn.00982.2011.

54. Mehaffey, W.H., Doiron, B., Maler, L., and Turner, R.W. (2005). Deterministic multiplicative gain control with active dendrites. J. Neurosci. *25*, 9968–9977. https://doi.org/10.1523/JNEUROSCI.2682-05.2005.

55. Tzounopoulos, T., Kim, Y., Oertel, D., and Trussell, L.O. (2004). Cell-specific, spike timing-dependent plasticities in the dorsal cochlear nucleus. Nat. Neurosci. *7*, 719–725.

56. Kim, Y., and Trussell, L.O. (2007). Ion channels generating complex spikes in cartwheel cells of the dorsal cochlear nucleus. J. Neurophysiol. *97*, 1705–1725.

57. Zhang, S., and Oertel, D. (1993). Cartwheel and superficial stellate cells of the dorsal cochlear nucleus of mice: intracellular recordings in slices. J. Neurophysiol. *69*, 1384–1397.

58. Singla, S., Dempsey, C., Warren, R., Enikolopov, A.G., and Sawtell, N.B. (2017). A cerebellum-like circuit in the auditory system cancels responses to self-generated sounds. Nat. Neurosci. *20*, 943–950. https://doi.org/10.1038/nn.4567.

59. Gao, Z., van Beugen, B.J., and De Zeeuw, C.I. (2012). Distributed synergistic plasticity and cerebellar learning. Nat. Rev. Neurosci. *13*, 619–635.

60. Perez, S., Cui, Y., Vignoud, G., Perrin, E., Mendes, A., Zheng, Z., Touboul, J., and Venance, L. (2022). Striatum expresses region-specific plasticity consistent with distinct memory abilities. Cell Rep. *38*, 110521. https://doi.org/10.1016/j.celrep.2022.110521.

61. Letzkus, J.J., Kampa, B.M., and Stuart, G.J. (2006). Learning rules for spike timing-dependent plasticity depend on dendritic synapse location. J. Neurosci. *26*, 10420–10429. https://doi.org/10.1523/JNEUROSCI.2650-06.2006.

62. Ruan, H., Saur, T., and Yao, W.D. (2014). Dopamine-enabled anti-Hebbian timing-dependent plasticity in prefrontal circuitry. Front. Neural Circuits *8*, 38. https://doi.org/10.3389/fncir.2014.00038.

63. Barlow, H.B. (1961). Possible principles underlying the transformations of sensory messages. Sens. Commun. 217–234.

64. Carnevale, N.T., and Hines, M.L. (2006). The NEURON Book (Cambridge University Press).

65. Sawtell, N.B. (2010). Multimodal integration in granule cells as a basis for associative plasticity and sensory prediction in a cerebellum-like circuit. Neuron *66*, 573–584.

66. Destexhe, A., Mainen, Z.F., and Sejnowski, T.J. (1994). An efficient method for computing synaptic conductances based on a kinetic-model of receptor-binding. Neural Comput. *6*, 14–18. https://doi.org/10.1162/neco.1994.6.1.14.

STAR★METHODS

KEY RESOURCES TABLE

REAGENT or RESOURCE	SOURCE	IDENTIFIER
Deposited data		
Raw and analyzed data	This paper; Mendeley Data	https://doi.org/10.17632/47nsb6x7nr.1
MG Cell morphology, simulation and analysis code of biophysical model	This paper and Muller et al. (2019)[12]; ModelDB	ModelDB: http://modeldb.yale.edu/267596
Experimental models: Organisms/strains		
Gnathonemus petersii	Wild-born fish caught in Africa	N/A
Software and algorithms		
Spike2	Cambridge Electronic Design	http://ced.co.uk/
MATLAB	MathWorks	https://www.mathworks.com
NEURON	Carnevale and Hines (2006)[64]	https://www.neuron.yale.edu/neuron/
Python3	Python	https://www.python.org/

RESOURCE AVAILABILITY

Lead contact

Further information and requests for data should be directed to and will be fulfilled by the Lead Contact, Nate Sawtell (ns2635@columbia.edu).

Materials availability

This study did not generate new unique materials.

Data and code availability

- Model code is available at: ModelDB: http://modeldb.yale.edu/267596
- Data and data code are available at Mendeley Data: https://doi.org/10.17632/47nsb6x7nr.1

EXPERIMENTAL MODEL AND SUBJECT DETAILS

Male and female Mormyrid fish (7-12 cm in length) of the species *Gnathonemus petersii* were used in these experiments. Fish were housed in 60 gallon tanks in groups of 5-20. Water conductivity was maintained between 40-65 microsiemens. All experiments performed in this study adhere to the American Physiological Society's *Guiding Principles in the Care and Use of Animals* and were approved by the Institutional Animal Care and Use Committee of Columbia University.

For surgery to expose the brain for recording, fish were anesthetized (MS:222, 1:25,000) and held against a foam pad. Skin on the dorsal surface of the head was removed and a long-lasting local anesthetic (0.75% Bupivacaine) was applied to the wound margins. A plastic rod was cemented to the anterior portion of the skull to secure the head. The posterior portion of the skull overlying the ELL was removed and the valvula cerebelli was reflected laterally to expose the eminentia granularis posterior (EGp) and the molecular layer of the ELL, facilitating whole-cell recordings from the ventrolateral zone of the ELL. Gallamine triethiodide (Flaxedil) was given at the end of the surgery ($\sim$20 μg/cm of body length) and the anesthetic was removed. Aerated water was passed over the fish's gills for respiration. Paralysis blocks the effect of electromotoneurons on the electric organ, preventing the EOD, but the motor command signal that would normally elicit an EOD continues to be emitted at a rate of 2 to 5 Hz.

METHOD DETAILS

Electrophysiology

The EOD motor command signal was recorded with a Ag-AgCl electrode placed over the electric organ. The command signal is the synchronized volley of electromotoneurons that would normally elicit an EOD in the absence of neuromuscular blockade. The command signal lasts about 3 ms and consists of a small negative wave followed by three larger biphasic waves. Onset of EOD command

was defined as the negative peak of the first large biphasic wave in the command signal. For pairing experiments, the EOD mimic was presented 4.5 ms following EOD command onset. Recordings were started ~1 hour after paralysis.

Methods for *in vivo* whole-cell recordings were the same as in prior studies of the mormyrid ELL.[12,65] Briefly, electrodes (8-15 MΩ) were filled with an internal solution containing, in mM: K-gluconate (122); KCl (7); HEPES (10); Na2GTP (0.4); MgATP (4); EGTA (0.5), and 0.5-1% biocytin (pH 7.2, 280-290 mOsm). No correction was made for liquid junction potentials. Membrane potentials were recorded and filtered at 10 kHz (Axoclamp 2B amplifier, Axon Instruments) and digitized at 20 kHz (CED micro1401 hardware and Spike2 software; Cambridge Electronics Design, Cambridge, UK). Only cells with stable membrane potentials more hyperpolarized than -40 mV and broad spike amplitudes >40 mV were analyzed. In contrast to broad spikes, narrow spike amplitude varied across recordings from ~15 mV (similar to values obtained from somatic recordings *in vitro*) to indistinguishable from subthreshold synaptic events. The latter, which were typically obtained at more superficial recording depths corresponding to the ELL molecular layer, were classified as putative apical dendritic recordings (see Figure S1D).

Electrosensory stimulation

The EOD mimic was a 0.2 ms duration square pulse delivered between an electrode in the stomach and another positioned near the electric organ in the tail. The amplitude was 25-50 μA at the output of the stimulus isolation unit (stomach electrode negative). Recordings from ampullary afferents showed that firing rate modulations evoked by this mimic are within the range of those induced by the fish's natural EOD.[22] We use the terms sensory input or sensory response to refer to the effect of the mimicked electric field on the ELL. Because we do not include prey-like electric fields the sensory input we discuss is entirely predictable on the basis of the EOD command signal and is therefore entirely uninformative to and 'unwanted' by the fish. Thus, we consider a situation where the ELL attempts to cancel *all* of its sensory input. It is important to appreciate that, in a natural setting, the mechanisms we analyze would only cancel the predictable self-generated component of the sensory input, leaving the unpredictable inputs of interest to the fish intact. To isolate responses to sensory versus corollary discharge we analyzed periods in which sensory stimuli were delivered independent of the EOD motor command. In some cases, sensory responses were isolated from periods in which the sensory stimuli were paired with the EOD motor command by off-line subtraction of responses to the EOD motor command alone.

Biophysical model

The compartmental model was based on a morphological reconstructed MG cell and consisted of 78 compartments further divided into 230 segments.[12] Simulation of cell activity was done using NEURON software and a Python 3 wrapper.[64] Voltage gated Na+ and K+ channels inserted in the apical dendrites and axon are Hodgkin-Huxley type channels. Temperature was set to 20° Celsius. The attenuation of axonal spikes in the model arises simply due to the resistance between axonal and somatodendritic compartments and limiting the density of voltage gated channels at the axon initial segment (AIS). Voltage-gated channel conductances were adjusted (see below) to achieve the higher spike threshold for broad versus narrow spikes that is observed experimentally.

Values of biophysical parameters for the different compartments

	g_l (S/cm^2)	leakage reversal potential (mV)	axial resistance (Ωcm)	Capacitance (μF/cm^2)	$\overline{g}_{Na}$ (S/cm^2)	$\overline{g}_K$ (S/cm^2)
axon	0.0003	-65	100	1	4	0.5
AIS	0.0003	-65	100	1	0.168	0.05
apical	0.0003	-65	100	1	0.1	0.008
rest	0.0003	-65	100	1	0	0

In the table above, 'rest' includes the soma, the somatic-connected apical compartment and all basal dendrite compartments. g_l is leakage conductance. $\overline{g}_{Na}$, and $\overline{g}_K$ are the maximal conductances of the sodium and potassium channels, respectively.

To drive baseline spiking in the model cell (the condition we term *initial*), we injected Gaussian current noise into the soma (0.5 ms timesteps) with a standard deviation chosen to evoke ~50 Hz narrow spike firing and ~2 Hz broad spike firing. To drive excitatory and inhibitory responses we added synaptic conductances with properties resembling AMPA and GABA(A) receptors.[66] Reversal potential of the AMPA and GABA(A) conductances are 0 mV and -65 mV, respectively. The AMPA excitatory input was inserted into all apical dendrite compartments (49 compartments, 175 segments). The AMPA and GABA(A) inputs were constant, with each relevant compartment receiving a synaptic input with timing onset (in units of ms) $\sim \mathcal{N}(t_i, 5^2)$ where $t_i \in$ [0, 10, 20, 30 …. T] (we used T = 50000). For basal dendrites inhibition (21 compartments, 45 segments), conductance was 0.1 μS and excitatory conductance was 7.65e-5 μS. For somatic inhibition, conductance was 0.04 μS and excitatory conductance was 1.85e-5 μS. For apical inhibition, conductance was 0.01 μS and excitatory conductance was 7.1e-5 μS. Apical inhibition was inserted into proximal apical compartments (11 compartments, 19 segments) defined as those whose center is within 100 μm of the center of the soma. For the mixture of excitatory and inhibitory input into the basal dendrites (Figure 4C), inhibition conductance was 0.18 μS and excitatory conductance was 1e-3 μS. Cancellation of the mixture of inputs was achieved by adding AMPA into the apical dendrites and conductance was set to 7.8e-5 μS. A small Gaussian noise was added to the conductance of each synaptic input.

Dependence of somatic spike amplitude on synaptic conductance (analytical results)

Figures 2C and 2E show a reduction of the amplitude of the backpropagating narrow spike due to the introduction of an inhibitory synaptic conductance. To analyze this effect, we consider a conductance-based model of a somatic compartment connected to a spike-generating axon. The somatic membrane potential is described by

$$C_m\dot{V} = -g_l(V - E_l) - g_a(V - V_a(t)) - g_eV - g_i(V - E_i)$$

with c_m the specific membrane capacitance, g_l and E_l the leakage conductance and reversal potential, g_a the conductance from the axon to the soma, g_i and E_i the inhibitory conductance and reversal potential, and g_e the excitatory conductance (the excitatory reversal potential is set to 0). The axonal membrane potential, V_a, is,

$$V_a(t) = E + A_a\, exp\left(-\frac{t}{\tau_a}\right)$$

where A_a is the fixed amplitude of the axonal action potential and $E = (g_lE_l + g_iE_i)/(g_l+g_e+g_i)$ is the resting potential of both the soma and axon. Note that we model the backpropagating action potential as decaying exponentially with fixed time constant τ_a from a peak voltage of $E + A_a$ to the equilibrium potential E. We assume that the membrane potential starts out at time 0 at the value $V(0) = E$. Then, for $t \geq 0$,

$$V(t) = E + \frac{g_a\tau_aA_a}{c_m(1 - r)}\left(exp\left(-\frac{t}{\tau}\right) - exp\left(-\frac{t}{\tau_a}\right)\right)$$

where $\tau = c_m/(g_l + g_a + g_e + g_i)$ and $r = \tau_a/\tau$.

From this, the peak of the backpropagating action potential in the soma occurs at time

$$t_{max} = \frac{\tau_a\, ln\,(r)}{r - 1}$$

and its amplitude $A = V(t_{max}) - E$ is

$$A = \frac{g_a\tau_aA_a}{c_m(1 - r)}(1 - r)r^{\left(\frac{r}{1-r}\right)} = \frac{g_a\tau_aA_a}{c_m}r^{\left(\frac{r}{1-r}\right)}$$

Any conductance increase, whether inhibitory or excitatory, will increase r, and the factor $r^{\left(\frac{r}{1-r}\right)}$ is a decreasing function of r. Thus, the backpropagating spike amplitude decreases when sensory evoked synaptic conductances are activated and increases if inhibitory or excitatory conductance decreases.

Two compartment model

Conductance based integrate-and-fire model was used for the two compartment model (Figure 4D). The equations for somatic and axonal membrane potential are:

$$c_m\dot{v_s} = -g_l(v_s - E_l) - g_i(v_s - E_i) - g_e(v_s - E_e) - g_c(v_s - v_a(t)) + I_e$$

$$c_m\dot{v_a} = -g_l(v_a - E_l) - g_c(v_a - v_s(t))$$

Where c_m is the specific membrane capacitance g_l is the leakage conductance, g_c is the intercompartment conductance and g_i and g_e are the inhibitory and excitatory conductances respectively. I_e is external current (with Gaussian noise) and is set to produce ~50 Hz narrow spike and ~2 Hz broad spike rates. When the axon reaches the threshold for axonal spike, a spike shape plus a refractory period (7ms) is imposed in the axon. Broad spike rate was determined by the number of times the backpropagating axonal spike reached a high threshold in the soma (this threshold was defined as the 97th percentile of the backpropagating spike-peak in the *initial* period). The shape of the added action potential = 1/2e-3 (exp(-t/0.3)-exp(-t/0.2))

Measuring narrow spike amplitude differences

Quantifying narrow spike amplitude differences induced by sensory input is complicated by the strong dependence of narrow spike amplitude on baseline membrane potential observed *in vivo* (negative slope in Figure 1I). To account for this effect, we fit the slope of the relationship between narrow spike amplitude and baseline membrane potential and report the difference across conditions in the bias of these slopes. Similarly, to measure difference between expected and actual amplitude (Figure S4A) we first fit a slope to the relationship between amplitude and baseline membrane potential across all periods and then measure the distance from the fit.

We hypothesize (Figures S1H and S1I) that the attenuation of the backpropagating narrow spike amplitude is linearly proportional to the amplitude:

$$AMP_2 = (1 - A)AMP_1$$

Where A is a constant representing attenuation, and subscripts 1 and 2 represent location relative to the soma where 1 is closer to the soma than 2. Thus, AMP_2 and AMP_1 represent amplitudes at compartments 2 and 1 respectively.

Then, if we divide by the average recorded mean we have the following equality:

$$\frac{AMP_1^{evoke} - AMP_1^{non-evoke}}{\text{mean}(AMP_1)} = \frac{(1-A)AMP_1^{evoke} - (1-A)AMP_1^{non-evoke}}{(1-A)\text{mean}(AMP_1)} = \frac{AMP_2^{evoke} - AMP_2^{non-evoke}}{\text{mean}(AMP_2)}$$

The average narrow spike amplitude differs widely across recordings (see Figure S1D), presumably due to recording location in the soma versus the proximal apical dendrites. Hence, to compare differences in narrow spike amplitude evoked by sensory stimuli across recordings we report the percentage change in narrow spike amplitude relative to the average narrow spike amplitude for each cell. The same reasoning applies to analysis of the relationship between amplitude and baseline membrane potential across different cells (Figure S4A).

F-I curve for narrow spikes

The fit between membrane potential and spike rate is approximately linear (see example in Figure 3E). To minimize the effect of outliers we quantify the change in rate/mV as:

$$\frac{\max(N\text{spk rate}) - \min(N\text{spk rate})}{\max(MP) - \min(MP)}$$

Determining windows of interest in Figure 3

As expected based on the recorded responses of ampullary afferents to brief (EOD-like) electrosensory stimuli,[22] peak modulation of broad spikes rate was observed 10-50 ms following the electrosensory stimulus. Thus, we limited the search for peak and trough broad spike responses to this window. For each period, we calculated average broad spike rate after smoothing with a 10 ms gaussian kernel. If peak broad spike response within 10-50 ms following the stimulus time was larger than 3 Hz, we defined the excitatory response window to be from 10 ms before to 5 ms following the broad spike peak response and analyzed amplitude and baseline membrane potential of narrow spikes within this window. Inhibitory responses were quantified in a 15 ms window following the initial stimulus-locked decrease in broad spike rate defined as reaching 0 broad spike rate. As the broad spike responses to electrosensory stimulus were minimal after 120 ms, we defined a period 120-160 ms after the stimulus as the 'unmodulated' window. For the 'control' analysis in Figure 3C, we compared amplitude and baseline membrane potential of narrow spikes occurring in windows 120-140 ms versus 140-160 ms after the stimulus. For 'late' and 'early' analysis in Figure 3D, we analyzed periods in which electrosensory input was paired with the EOD at least 300 times and then defined the last 100 trials as 'late' and first 100 as 'early' to measure the changes resulting from the pairing.

Measuring *in vivo* changes due to cancellation (Figure 3D)

The recorded peak, amplitude and baseline membrane potential of *in vivo* narrow spikes may change over the course of the recording (e.g. due to changes in recording quality). Therefore, we measured differences relative to a control window within the same recording period:

$$\text{late} - \text{early} = (\text{test window} - \text{control window})(\text{late}) - (\text{test window} - \text{control window})(\text{early})$$

QUANTIFICATION AND STATISTICAL ANALYSIS

Software used and general statistical methods

Data were analyzed off-line using Spike2 (Cambridge Electronic Design) and custom Matlab code (Mathworks, Natick, MA). Biophysical model analysis was performed using custom Python3 code. Non-parametric tests were used for testing statistical significance. Unless otherwise indicated, we used the two-sided Wilcoxon rank sum test for unpaired samples and the Wilcoxon signed ranks test for paired samples. Differences were considered significant at $P < 0.05$. 3 stars indicate a $P < 0.001$